Results in Engineering 27 (2025) 106144

Contents lists available at ScienceDirect

Results in Engineering

journal homepage: www.sciencedirect.com/journal/results-in-engineering

Research paper

Effect of fiber-matrix interaction and embedment length on the pullout behavior of rice straw fibers embedded in clay matrix

Oswaldo Hurtado-Figueroa [a,d,*], Humberto Varum [b], María Isabel Prieto [c], Romel J Gallardo Amaya [d], Alfonso Cobo Escamilla [a]

[a] Escuela Técnica Superior de Edificación, Universidad Politécnica de Madrid—UPM, 28040 Madrid, España
[b] CONSTRUCT-LESE, Departamento de Engenharia Civil, Faculdade de Engenharia da Universidade do Porto, FEUP, 4200-465 Porto, Portugal
[c] Departamento de Tecnología de la Edificación, Universidad Politécnica de Madrid—UPM, 28040 Madrid, España
[d] Grupo de Investigación en Construcción, Geotecnia y Medio Ambiente—GIGMA, Universidad Francisco de Paula Santander Ocaña—UFPSO, 546552 Ocaña, Colombia

ARTICLE INFO

Keywords:
Rice straw
Clay matrix
Fiber-matrix interaction
Single-fiber pullout test
Alkaline treatment

ABSTRACT

Earth as a building material is considered an environmentally friendly alternative for implementation in modern construction. The improvement of mixtures with clay matrix presents advances in their mechanical resistance by adding vegetable fibers as reinforcement. Some research concludes its results based on destructive testing without a thorough analysis of fiber-matrix interaction. In the present study, fiber-matrix interaction phenomena were analyzed using the single-fiber pullout test. The test was performed on rice straw fibers mercerized in 1 %, 2 %, and 3 % NaOH solutions embedded 5 mm, 10 mm, and 15 mm in a clay matrix stabilized with Carboxymethylcellulose and Cassava starch. The importance of NaOH treatment improving the surface roughness of the fibers was demonstrated. The surface modification favored the adhesion of the matrix to the fiber causing opposition to detachment. The geometrical irregularities of some fibers caused friction phenomena that required higher forces than those exerted in the initial detachment. The fibers treated in 1 % NaOH solution with an exposure time of 1 hour and embedded for 10 mm showed higher initial detachment force and opposition to displacement due to friction phenomena. The rigidity of the straw treated with 2 % NaOH solution for 2 h prevented its confinement by shrinkage due to drying of the matrix, a phenomenon that facilitated its extraction due to minimal opposition to friction. The low bonding stress of the plant fibers with the clay matrix favors the semi-ductile behavior of the green composite The single-fiber pullout test on vegetable fibers embedded in clay matrixes allows for identifying the fiber-matrix interaction and the optimal working length.

1. Introduction

The current environmental pressure generated by the mass production of materials and the inadequate handling of waste elements opened a field of research that aims to combine materials to develop environmentally friendly composites with sustainable characteristics taking into account the mechanical properties necessary for their use [1].

The complexity and high costs of modifying the physicomechanical properties or characteristics of metallic and ceramic materials due to the energy expenditure required for their transformation and interaction with other elements and the difficulty of their separation, rule them out for use as matrices in the formation of composites with sustainable characteristics [2]. For this reason, polymeric materials are presented as a viable alternative for the elaboration of composite materials due to their ease of molding with low energy consumption and their compatibility with any type of fiber that acts as the main reinforcement [3]. Reinforcing elements of which vegetable fibers are being used in

Abbreviations: Av, Average; CM, Control Mixture; CS, Compressive strength; DC, Degree of chalking; DS, Drying shrinkage; Ec, epidermal cells; EDS, Energy Dispersive Xray Spectroscopy; E-length, Embedded length; EMS, Experimental mixtures; ETAT, Exposure time in alkaline treatment; Ffr, Friction force released; Flh, Friction length; FS, Flexural strength; GD, Increase in density; Iff, Initial friction force); Itf, Initial tensile force; LV, Volume loss; MA, Moisture Absorption; Max, Maximum; Mff, Maximum friction forcé); Min, Minimum; N, Newton; Pfz, Primary friction zone; Pl, Papillae; Rfr, Removing fiber; RSS, Rice straw fibres; Sample-I, Sample identification; Sca, Silica-covered areas; SEM, Scanning Electron Microscopy; Sh, Single hair; τ, Bond stress; Tfr, Tensile force released; Uff, Ultimate friction force; Utf, Ultimate tensile force; Vff, Variation in friction forcé; Wx, Wax; %Vc, Coefficient of variation.

* Corresponding author at: Escuela Técnica Superior de Edificación, Universidad Politécnica de Madrid—UPM, 28040 Madrid, España.
E-mail addresses: os.hurtado@alumnos.upm.es (O. Hurtado-Figueroa), hvarum@fe.up.pt (H. Varum), mariaisabel.prieto@upm.es (M.I. Prieto), rjgallardoa@ufpso.edu.co (R.J.G. Amaya), alfonso.cobo@upm.es (A.C. Escamilla).

https://doi.org/10.1016/j.rineng.2025.106144
Received 23 May 2025; Received in revised form 3 July 2025; Accepted 4 July 2025
Available online 5 July 2025

Nomenclature

$CH_3 - COOH$ Acetic acid
$NaOH$ Sodium hydroxide

multiple investigations due to their natural properties that allow their implementation in the elaboration of composite materials with sustainable characteristics. Composite materials are also called Green composites [4].

However, the use of fossil fuels as the main element in the manufacture of a large part of polymeric materials is pointed out as a direct cause of greenhouse gas emissions due to the energy costs in their processes and waste inherent in the manufacture of the material [5]. However, the manufacture of polymeric materials is moving away from its dependence on oil to reduce the pollution footprint generated both in the manufacturing process and in the final disposal of the elements after their useful life [6]. Multiple research has presented advances in the development of fully biodegradable green resins from crops demonstrating the ability to replace dependence on petroleum [7].

In order to save energy costs concerning the processing of new materials, alternative matrices are being implemented to meet the needs of different industrial sectors, especially the construction industry [8]. Such is the case of clayey earth, a natural element used ancestrally as a building material in ancient societies, whose traces show the physicomechanical properties of the material over time [9]. The use of clay earth as a building material has accompanied man in his evolution as the main element for the construction of shelters and dwellings. Mixtures made from this natural material show considerable strengths through primitive additions of which vegetable fibers make up the main structure that increases its resistance to external stresses [10].

The ancestral construction techniques such as the Earth brick [11], Wattle and daud [12], Cob [13], and direct application mixtures such as plasters of which clayey earth is the main material, have used vegetable fibers as reinforcement elements to improve their physicomechanical characteristics by increasing the mechanical resistance of the elaborated elements. If vegetable fibers are to be used as reinforcing elements in the production of Green composites with particular mechanical properties, the origin of the fiber must be carefully chosen. That is, diversity, cultivation process, climatic conditions, and post-harvest harvesting, among other factors, can compromise the mechanical properties of vegetable fibers due to their natural origin. These compositional and handling factors account for its main quality characteristics and mechanical diversity [14].

However, the surface of the vegetable fibers can be modified to alter their compatibility with the matrix and improve the mechanical strength of the Green composite. These modifications can be made by physical or chemical treatments that increase fiber-matrix interaction by improving surface topography. These characteristics are decisive for the final mechanical properties of the Green composite [15]. Physical treatment is carried out by mechanical action that modifies the size of the fiber and improves its roughness. Chemical treatments, on the other hand, react with the structure of the cell wall, modifying its chemical composition by eliminating lignin, hemicellulose, pectin, waxes, and impurities, among other elements present on its surface. Characteristics increase the roughness of vegetable fibers and increase their tensile strength and elongation [16].

This property enhancement classifies chemical treatments as the best option for modifying the surface topography of vegetable fibers and improving their mechanical properties. Chemical treatments improve interfacial adhesion between the fiber and the matrix by increasing load transfer [17].

The main objective of the present research was to experimentally perform a single fiber pullout test on mercerized rice straw embedded in clay matrix. This research work has been developed by the main author in his doctoral thesis, the results of which have been previously published and are part of the references of this manuscript.

1.1. Alkaline treatment (NaOH)

The alkaline treatment or mercerization process is presented as an easy and inexpensive chemical procedure that alters the cell wall of vegetable fibers by decreasing their moisture absorption capacity. The process consists of immersing the vegetable fibers in a solution of sodium hydroxide (NaOH) in distilled water [18].

NaOH dissolves hemicellulose, the hydrophilic building block polymer present in the fiber structure, reducing its moisture absorption. The alkaline treatment also removes lignin, a key polymer in vegetable fibers that facilitates stiffening and bonding between cellulose fibers. Lignin removal causes roughness in the surface topography of the fibers due to the exposure of the cellulose microfibrils. Similarly, alkaline treatment causes the removal of wax and impurities. A phenomenon that causes surface roughness allowing interfacial adhesion favoring fiber-matrix interaction [19].

However, due to the aggressiveness of the alkaline treatment, it must be controlled to avoid irreparable damage to the vegetable fibers. High NaOH concentrations and long fiber exposure times in the alkaline treatment cause excessive lignin removal. This phenomenon promotes the detachment of cellulose microfibrils, considerably affecting their mechanical properties [20].

1.2. Vegetable fibers in clay matrixes

Several researches have implemented the use of vegetable fibers in clay matrixes to improve the physicomechanical characteristics of raw earth-based elements or mixtures. The research's aims to stabilize the clay matrix by adding vegetable fibers as reinforcement element.

Research has implemented the use of various vegetable fibers to stabilize the clayey earth to improve its physicomechanical properties. This type of stabilization focuses on counteracting the appearance of cracks caused by moisture loss, drying shrinkage, application of external forces, temperature changes, and other phenomena directly involved in the cracking of mixtures with a clayey matrix [21].

Improving the crack resistance of clay matrix mixtures through the use of lignocellulosic fibers increases the likelihood of their application as a material in modern construction works. This feature gives comparative environmental advantages in contrast to other types of fibers due to their plant origin, low cost, and renewability [22].

In the study by Ojo et al. [23], the authors used Sisal fibers to stabilize mixtures with clay matrix in the elaboration of construction elements manufactured by the extrusion process. The authors concluded that the addition of vegetable fibers significantly modified the blends by improving packing density through extrusion effects. The packing density reduced the moisture absorption of the mixture due to fiber-matrix interaction. The occurrence of cracks was significantly reduced due to the interfacial bonding of the components. The added fiber increased the modulus of rupture by 74 % compared to the results of the non-stabilized mixture.

In the research carried out by Araya-Letelier et al. [24], the authors improved the physicomechanical properties of earth brick by incorporating jute fibers in additions of 0.5 % and 2 % by weight and fiber lengths of 7 mm, 15 mm, and 30 mm. The authors concluded that additions $\geq$ 2 %, regardless of fiber length, increase capillary moisture absorption. On the other hand, additions of 2 % fibers with a length of 15 mm significantly decreased the occurrence of cracks in the drying process. Similarly, the addition of 2 % fiber increased the mechanical strength of the mixes. The research determined that the critical fiber length was 15 mm because, in mixes with 0.5 % fiber additions, increased mechanical strength was noted through reduced cracking.

In the research work by AlShuhail et al. [25] the authors used date

palm fibers and wood chips to improve the performance of earth blocks. The authors concluded that the impact of date palm fibers on the mechanical behavior of the mixtures was superior compared to wood chips. Moisture absorption was lower in mixtures with the addition of this type of fiber due to a considerable decrease in the occurrence of cracks. This feature prevented the generation of pores and improved the mechanical properties of the experimental mixtures.

In the study by Salih et al. [26], the authors used sugar cane bagasse fibers in proportions of 1 %, 3 %, 5 %, 7 %, 7 %, 9 %, and 11 % by weight with lengths of 5 mm, 10 mm, 15 mm, and 20 mm. The research concluded that the earth bricks with the addition of 5 % fibers increased the compressive strength by 78.7 % compared to the control mixtures. This increase in mechanical strength was due to the stabilization of the volume and crack control of the mixture by the addition of the fibers.

Fig. 1 shows the four typical behaviors of fibers in preventing crack propagation in a composite material. The figure shows fiber breakage due to over-anchoring with the matrix (I). Fiber elongation is shown as one of its physical properties (II). The detachment of the fiber due to lack of adhesion with the matrix (III) is shown. The opposition of the fiber to detachment with the matrix due to friction phenomena is shown (IV).

However, research that implements vegetable fibers as reinforcement elements in clay matrix mixtures lacks tests that demonstrate in detail the influence of fiber length and surface topography on fiber-matrix interaction. This type of interaction is based on adhesion phenomena between surfaces that occur when the composite material receives external loads. The point at which its mechanical stress begins.

It can be indicated that the mechanical resistance of the construction elements made from mixtures with clay matrix is subject to the properties of the vegetable fiber that acts as a reinforcement element. The characteristics of its origin, type of extraction, physical or chemical treatments, fiber length, and other particularities are presented as the comparative basis for its choice as a reinforcement element in future research [27].

However, testing the mechanical strength of experimental mixtures with clay matrix reinforced with vegetable fibers is subject to the elaboration of specimens that can add up to significant quantities affecting the estimated time of the research and the financial resources allocated in its budget [28].

The implementation of research methods to identify the individual characteristics of vegetable fibers intended to be used as reinforcement elements in mixtures with a clay matrix favors the direction of the research to advance in results, optimizing resources and leading to a reduction in time and budget.

In response, the single-fiber pullout test is presented. This test allows the determination of the bond strength and the critical length of the reinforcement fiber by evaluating the bond strength per unit area of the fiber in contact with the matrix [29].

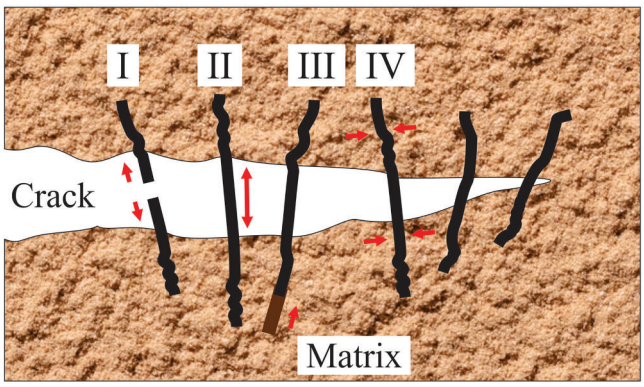

Fig. 1. Behavior of fibers under cracking. (I) Breakage, (II) Elongation, (III) Detachment, (IV) Friction.

1.3. Single-fiber pullout test

The single-fiber pullout test consists of making a sample with typical test characteristics in which 50 % of the length of the fiber to be used as a reinforcement element is embedded, leaving a free length of the fiber. Tension force is then applied to the free end of the fiber and the data for pullout force and displacement are recorded [30]. The purpose of the test is to determine the maximum force required for the detachment of the fiber and to evaluate the force exerted in the section corresponding to its extraction.

Although the single-fiber pullout test is commonly performed on fibers or metallic elements embedded in a cementitious matrix, this test can be applied experimentally to understand the interfacial behavior of vegetable fibers embedded in a clay matrix.

Fig. 2 shows the set-up of the single-fiber pullout test performed in this research. The figure shows the test's general characteristics to evaluate the rice straw's adhesion to the clay matrix. Fig. 2a shows the tension clamps (I). Specimen (II). Rice straw fiber (III). The jaw gripping system is shown (IV). Fig. 2b shows the fiber length embedded in the clay matrix (V). The displacement of the embedded fiber due to the applied force is shown (VI). The applied tensile force is shown (VII).

Knowing the fiber-matrix adhesion tension facilitates the identification of the optimal fiber length and the behavior of its surface topography when interacting with the matrix to prevent its extraction. This information makes it possible to identify the interfacial bonding of the components by determining their mechanical behavior under stress [31].

Generally speaking, it can be stated that in the single-fiber pullout test, a two-stage process takes place. The first stage consists of fiber breakage or detachment caused by the degree of adhesion between the fiber and the matrix. This phenomenon is caused by the force exerted when extracting the fiber. At this stage, resistance to initial fiber extraction is the responsibility of the fiber-matrix interaction [32].

The second stage consists of the displacement of the fiber before it is completely removed from the matrix. After detachment of the fiber, the force exerted causes the fiber to move to be extracted. At this stage, it can be indicated that the slip resistance of the fiber is caused by frictional effects [33].

Fig. 3 presents the possible causes of friction effects between the clay matrix and the vegetable fibers. The black arrows represent the applied tensile force. The red arrows represent the frictional force exerted. The green arrows represent the external forces that cause the deformation of the vegetable fibers. Fig. 3a shows the friction generated by roughness in the surface topography of the fiber. Fig. 3b shows the friction that occurs due to the change in fiber axis caused by external pressures when processing the Green composite. Fig. 3c shows the friction generated by confining effects caused by drying shrinkage of the clay matrix. Fig. 3d shows the friction effect of the vegetable fiber due to its geometrical irregularity. Fig. 3e shows the friction caused by mechanical locking resulting in the detachment of particles from the clay matrix.

Determining the optimum length of the vegetable fiber and its level of adhesion to the clay matrix avoids costs and delays in specimen preparation and testing. This activity allows for the advancement of research into the elaboration of mixtures that will give rise to construction elements based on raw earth.

Incorporating ancestral building methods into modern architecture provides alternatives to the growing need for clean and sustainable production. However, it must be considered that the mechanical properties of the raw earth-based building material or element must be within the admissible parameters of the regulations in force [34]. Characteristic underpinning the importance of testing before the manufacture of Green composite made of clay matrix reinforced with vegetable fiber [35].

The main objective of the present research was to identify the optimum embedment length and the incidence of fiber-clay matrix interaction on the pullout resistance of rice straw fibers. The research used

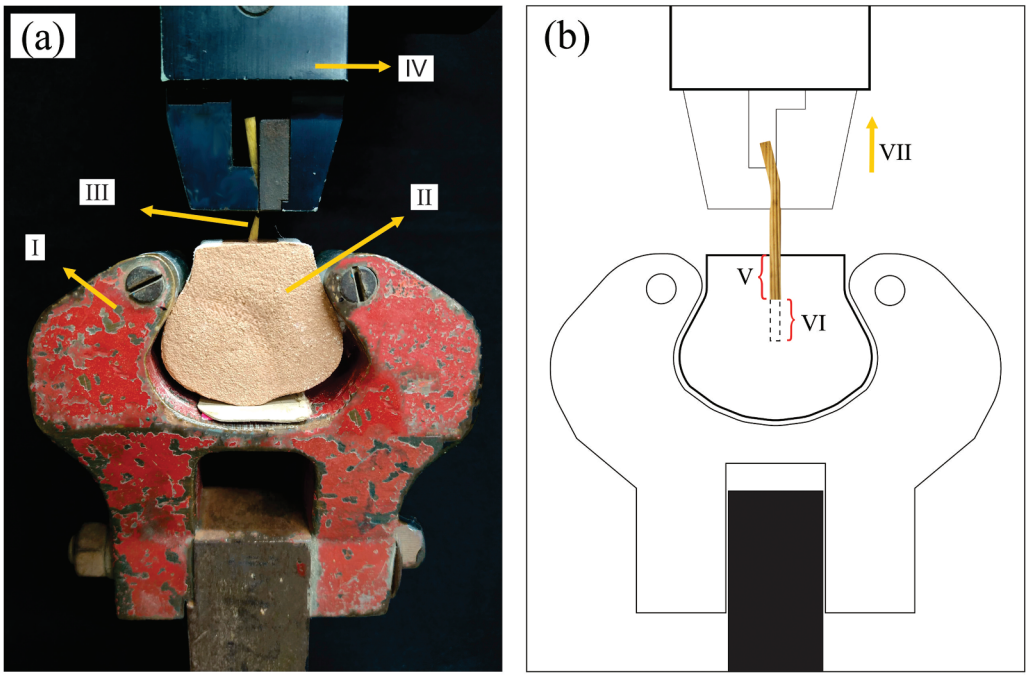

Fig. 2. Single-fiber pullout test. (a) Test set-up, (b) Fiber displacement under tensile force.

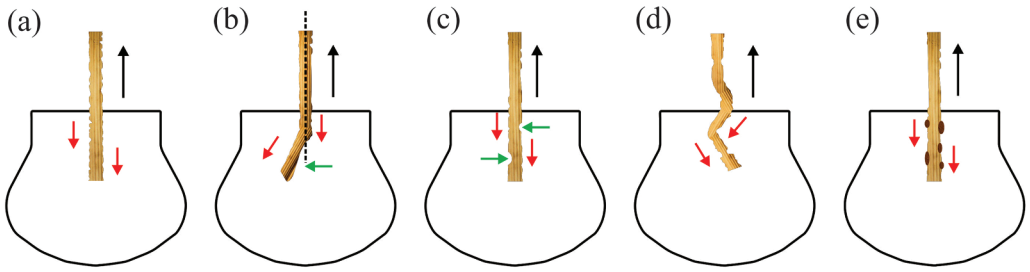

Fig. 3. Friction phenomena vegetable fiber-clay matrix. (a) Roughness, (b) Axis change, (c) Confinement, (d) Irregular geometry, (e) Particle detachment.

mercerized rice straw fibers embedded 5 mm, 10 mm, and 15 mm in a clay matrix stabilized with Carboxymethylcellulose and cassava starch. The process implemented was the single-fiber pullout test. A method commonly used to determine the pullout behavior of metallic elements or fibers embedded in portland cement-based matrixes [36].

The development of the research allowed us to describe in detail the phenomena that occurred in the single-fiber pullout test applied to rice straw fibers embedded in a clay matrix. The physical characteristics of the fibers for the production of Green composites with clay matrixes were identified based on the evaluation of the adhesion tension presented in each of the samples analyzed. The research generated scientific data on the behavior of the interaction of mercerized rice straw fibers with the clay matrix under tensile stress.

The detailed description of the processes carried out in the present investigation serves as a reference base for future investigations in which the use of vegetable fibers as a reinforcement element in mixtures with a clay matrix is intended. The application of the single-fiber pullout test in future research avoids the excessive production of destructive test specimens to determine the mechanical behavior of experimental mixtures. Feature that considerably reduces costs and estimated research times.

2. Materials and methods

2.1. Material

The materials used in the single-fiber pullout test were selected from previous research published by the authors of this article. Based on the published results, the rice straw fibers and the clay matrix were selected according to the most suitable physical and mechanical criteria.

2.1.1. Rice straw

Rice straw fibers were used based on data published by Hurtado Figueroa et al. [20] in the article entitled "*The Mercerization Process and Its Impact on Rice Straw Surface Topography*". Four types of rice straw fibers (RSS) were selected. RSS without mercerization process (RSS-3W/ut) which served for comparison. RSS mercerized in 1 % NaOH solution immersed for 1 h (NaOH 1 %/1 h). RSS mercerized in 2 % NaOH solution immersed for 2 h (NaOH 2 %/2 h). RSS mercerized in 3 % NaOH solution immersed for 1 h (NaOH 3 %/1 h). The criteria for the selection of RSS were the results obtained in the tensile and elongation tests.

Table 1 presents the results of the stress and elongation test published in the article " *The Mercerization Process and Its Impact on Rice Straw Surface Topography*". The table where the fibers used in the present research were selected. The table shows the average (*Av*) of the results after testing 10 samples for each of the RSS. The results obtained in the tension tests were valued in Newton (N) and the elongation data was

Table 1
Tensile and elongation test RSS [20].

RSS	Tensile N				Elongation%			
	Av	%Vc	Max	Min	*Av*	%Vc	Max	Min
RSS-1	78	46.66	171.3	43.2	2.5	38.82	4.4	1.5
RSS-2	105.1	15.28	121.1	79.7	2.6	16.49	3.3	1.9
RSS-3 W/Ut	83.7	26.54	117	59.5	3.9	33.85	6.6	2.7
NaOH 1 % 1h	68	30.05	97.3	42.6	4.4	27.77	6	1.9
NaOH 1 % 2h	37.3	31.87	60.8	25.3	3.8	23.60	5	2.7
NaOH 1 % 3h	49.1	39.25	92.2	32.9	4.8	23.92	6.4	2.6
NaOH 2 % 1h	45	37.82	68	21.3	5	33.15	7.5	2.8
NaOH 2 % 2h	59.7	31.1	88.5	25.5	5.1	33.07	7.9	2.2
NaOH 2 % 3h	37.3	30.17	56.1	18.7	4.6	25.35	6.6	2.2
NaOH 3 % 1h	36.1	44.43	78.3	22.1	5.6	37.34	10.3	2.7
NaOH 3 % 2h	27.4	39.01	45.6	11.4	5.2	33.38	8.6	2.7
NaOH 3 % 3h	32.7	24.62	48.7	24.3	5.3	26.25	8.2	3.8

valued in % concerning the length of the RSS samples analyzed. The coefficient of variation (%Vc) indicated the measure of dispersion of the data that allowed the analysis of their deviations. The maximum (Max) and minimum (Min) values show the highest and lowest results for each of the tests [20].

2.1.2. Clay matrix

The clay matrix used in the single-fiber pullout test was selected from the article published by authors Hurtado-Figueroa et al. [37] "*Effect of cassava starch, hydrated lime, and carboxymethylcellulose on the physicomechanical behavior of mixtures with clay matrix*". The matrix selection criteria consisted of the results obtained in the compressive strength (CS), flexural strength (FS), and degree of chalking (DC) tests. The selected matrix was the EMS-30. The clay matrix consists of 97 % clay stabilized with 0.75 % cassava starch and 2.25 % carboxymethylcellulose. The mixture was moistened with 40 % by weight of mixing water.

Table 2 presents the results of the physical and mechanical tests of the clay matrixes published in the article "*Effect of cassava starch, hydrated lime, and carboxymethylcellulose on the physicomechanical behavior of mixtures with clay matrix*". The table where the matrix used in this research was selected. The table shows the results of the control mixture (CM) and experimental mixtures (EMS). The DC is shown where No. 2 corresponds to a high degree of particle detachment and No. 8 corresponds to no particle detachment. The percentage increase in matrix density (GD) is presented. Volume loss (LV). Drying shrinkage (DS) and moisture absorption by capillarity (MA). Values are shown for CS and FS [37].

2.2. Methods

2.2.1. Mold manufacturing

The mold for the single-fiber pullout test was made using the dog-bone-shape described in the Standard Test Method for Tensile Strength of Chemical-Resistant Mortar, Grouts, and Monolithic Surfacings ASTM C307–23 [38]. The Molds corresponding to half of the dog bone shape were made. However, the mold dimensions were modified due to the volumetric variation of the EMS-30 after 40 days of shade drying, the time during which the samples were tested (see Table 2). To complement the mold, a piece of transparent acrylic was made with a central perforation to allow the RSS to enter the mold.

Fig. 4 shows the fabrication of the molds for the single-fiber pullout test. Fig. 4a shows the dimensions of the original mold according to ASTM-C307–23 [38]. Fig. 4b shows the mold with the dimensions modified in the investigation according to the physical characteristics of the matrix. (see Table 2). Fig. 4c shows the mold manufactured.

2.2.2. Samples preparation

For the preparation of the samples, 3 lengths of RSS were determined. 10 mm, 20 mm 30 mm, these lengths were selected based on the results reported in research by Omrani et al. [39], Mazhar Syed & Anasua GuhaRay [40], Ojo et al. [23], Salih et al. [26]. The chosen lengths correspond to the working length of the fibers added as reinforcement elements in the experimental mixtures of the investigations used as references. However, for the single-fiber pullout test, 50 % of the working length of the fiber was embedded in the matrix. That is, for the 10 mm RSS, 5 mm was embedded in the clay matrix. For the 20 mm RSS, 10 mm was embedded and for the 30 mm RSS, 15 mm was embedded.

The clay matrix mixture was prepared with 97 % clay stabilized with 0.75 % cassava starch and 2.25 % carboxymethylcellulose. The mixture was wetted with 40 % by weight of distilled water. The mixture was elaborated by mechanical process [37]. The mixture was poured into the mold by hand and then screeded. The position of the fiber was guaranteed using the acrylic slice (see Fig. 5).

The samples were identified according to the NaOH concentration, the exposure time of the RSS in the alkaline treatment, and the embedded length of the RSS. For RSS that was treated in 1 % NaOH immersed 1 h with 5 mm of embedded fiber, it was identified as NaOH 1 %/1h-0.5. The other samples were identified in the same way. The untreated RSS did not show any alkaline treatment in its identification.

Table 3 shows the identification of each of the samples tested. The table shows the NaOH concentration (NaOH %). RSS exposure time in alkaline treatment (ETAT). Embedded length (E-length) and, sample

Table 2
CM and EMS physicomechanical test results [37].

Mixures	Physical tests								Mechanical test	
	DC				%				kgf/cm^2	
	No. 8	No. 6	No. 4	No. 2	GD	LV	DS	MA	CS	FS
CM	–	–	X	–	10.11	27.24	9.31	1.76	54.06	17.85
EMS-48	–	X	–	–	50.96	54.93	20.50	1.84	115.26	23.61
EMS-21	–	X	–	–	24.24	50.73	18.55	1.94	121.38	29.33
EMS-15	X	–	–	–	4.40	41.93	15.55	2.32	84.66	14.08
EMS-38	–	–	X	–	−18.69	23.09	14.06	8.87	73.44	25.55
EMS-41	–	X	–	–	1.73	33.80	9.87	3.36	89.76	27.54
EMS-28	–	X	–	–	12.94	36.16	13.87	1.56	51	13.18
EMS-35	–	–	–	X	6.33	32.75	10.70	2.9	46.92	15.10
EMS-45	X	–	–	–	6.33	34.69	11.35	4.69	87.72	22.70
EMS-30	X	–	–	–	8.58	36.07	13.40	3.14	80.58	78.50
EMS-2	–	–	–	X	6.50	29.45	9.77	7.6	27.54	6.53
EMS-42	X	–	–	–	3.94	37.81	12.92	3.31	87.72	59.82
EMS-4	–	–	–	X	5.82	26.14	8.56	4.13	36.72	9.03
EMS-39	–	–	–	X	13.94	34.47	12.09	6.27	54.06	5.05
EMS-11	–	–	–	X	17.61	33.74	10.70	2.13	51	10.66
EMS-24	–	–	X	–	37.02	47.39	17.47	3.26	86.7	22.54
EMS-33	–	–	–	X	−27.26	22.26	6.70	8.10	37.74	4.79

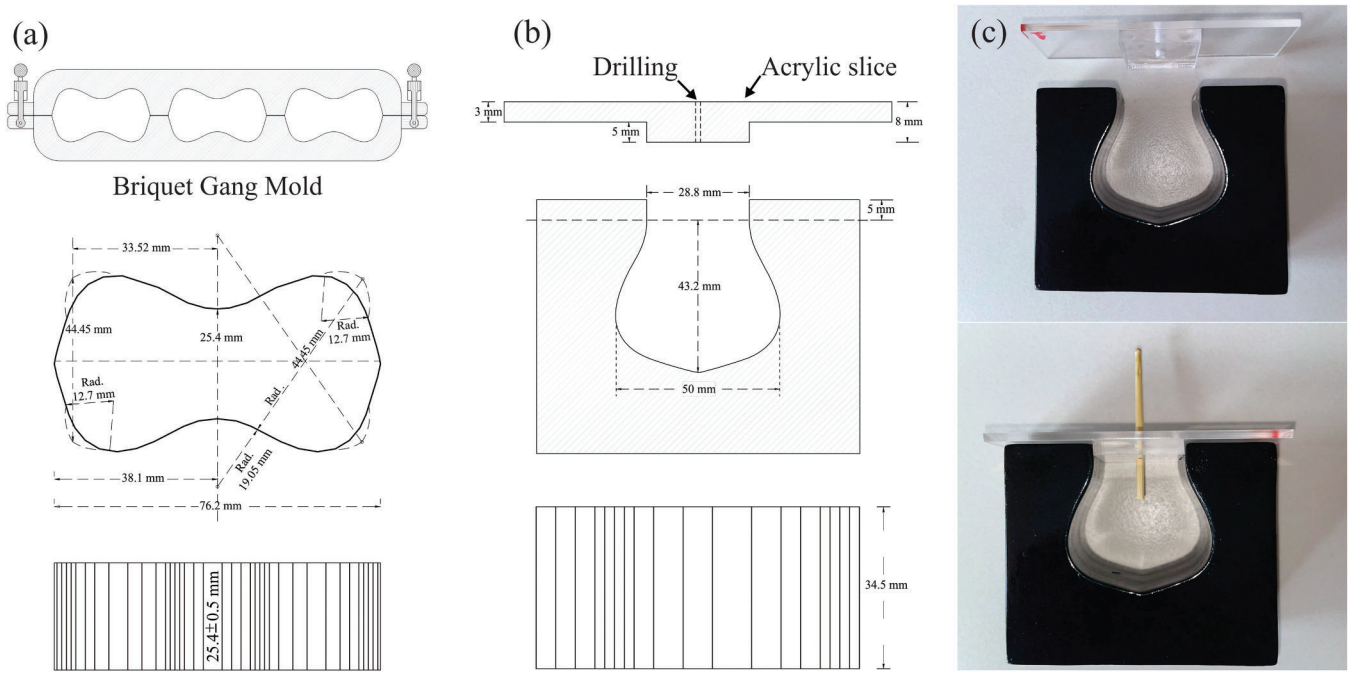

Fig. 4. Mold elaboration. (a) Mold with standard dimensions, (b) Mold with modified dimensions, (c) Fabricated mold.

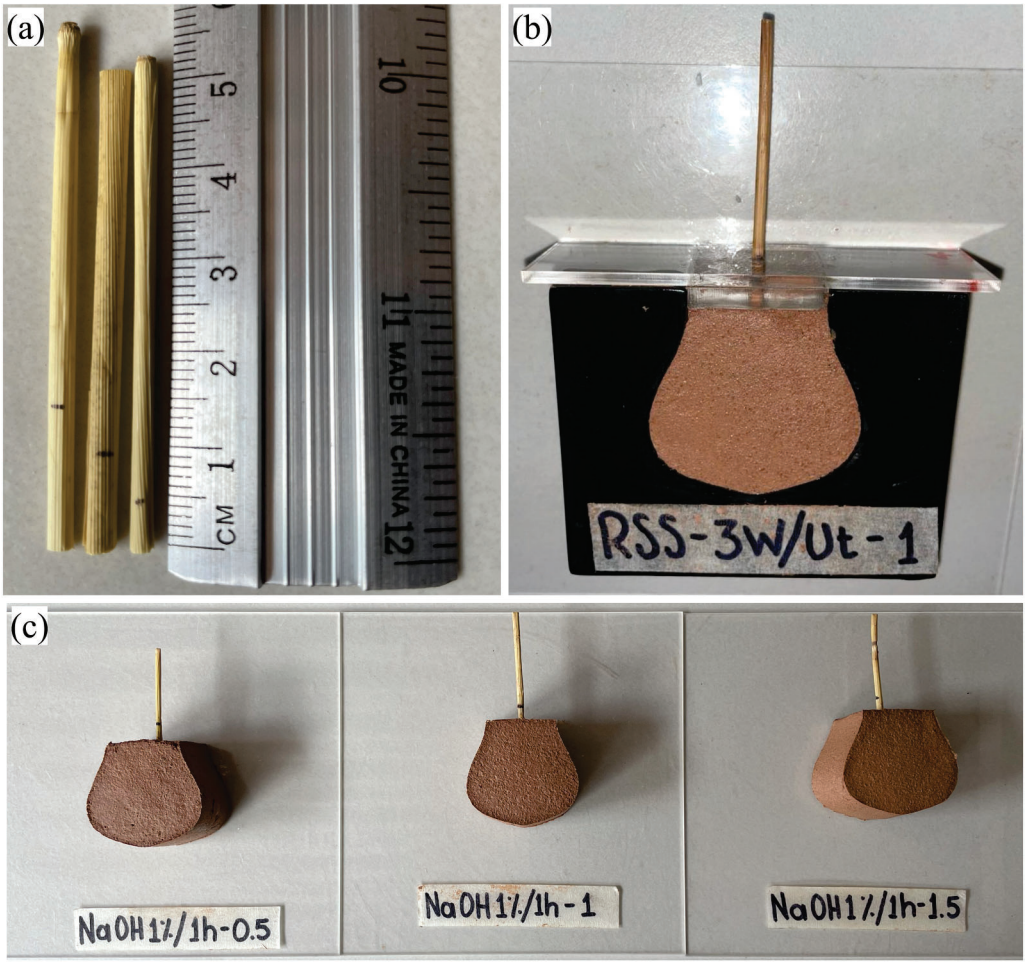

Fig. 5. Specimen preparation process. (a) Fiber length, (b) Specimen in mold, (c) Fabricated specimens.

Table 3
Sample identification.

NaOH (%)	ETAT (h)	E-length (mm)	Sample - I
–	–	5	RSS-3W/ut-0.5
		10	RSS-3W/ut-1
		15	RSS-3W/ut-1.5
1	1	5	NaOH 1 %/1h-0.5
		10	NaOH 1 %/1h-1
		15	NaOH 1 %/1h-1.5
2	2	5	NaOH 2 %/2h-0.5
		10	NaOH 2 %/2h-1
		15	NaOH 2 %/2h-1.5
3	1	5	NaOH 3 %/1h-0.5
		10	NaOH 3 %/1h-1
		15	NaOH 3 %/1h-1.5

identification (Sample-I). Three specimens were produced for each of the samples to average their results to ensure the accuracy of the data.

Fig. 5 shows the sample preparation process. Fig. 5a shows the lengths of RSS that were embedded. Fig. 5b shows the specimen inside the mold with the embedded fiber. Fig. 5c presents the processed samples with their respective identification.

2.2.3. Single-fiber pullout test

After 40 days of drying at room temperature, the single-fiber pullout test was carried out. The test was carried out by the laboratory of ceramic and composite materials of the School of Materials Engineering of the Universidad del Valle - Colombia. The test was performed on the Tinius Olsen machine. The load cell used in the test was 1 kN. The test speed was 1 mm/min [38].

Fig. 6 presents the process that was carried out in the single-fiber pullout test. Fig. 6a shows the samples before testing. Fig. 6b shows the mounting of the singles on the testing machine. Fig. 6c shows the test run. Fig. 6d shows the samples with the extracted fiber.

2.2.4. Scanning electron microscopy & energy dispersive X-Ray spectroscopy

Scanning electron microscopy (SEM) analysis was carried out to identify the adhesion phenomena of the mercerized fibers to the clay matrix. The analysis was carried out with the Jeol JSM 6010LA. The same equipment was used for the Energy Dispersive X-ray Spectroscopy (EDS) test. Mapping that identified the elemental chemistry of the surfaces analyzed. EDS mapping was able to determine the effects of the elemental chemistry of the samples on adhesion phenomena. The tests were carried out by the technological services laboratory of the Textile and Leather manufacturing center - SENA Bogotá.

3. Results and discussion

The single-fiber pullout test identified the adherence of the clay matrix to the RSS. This test allows us to predict the behavior of the fiber acting as reinforcement in a composite material after the fracture or cracking of the matrix at the moment of overcoming its breaking stress [41]. It is at this moment that the fiber acts as a link holding the ends of the crack, preventing it from advancing under subsequent stresses. This mechanical response of the reinforcement fiber is caused by its resistance to pullout. This action leads to a semi-ductile behavior of the composite material [42].

3.1. Effort evaluation

The fibers embedded in the clay matrix showed different behaviors when extracted. Behaviors were assessed by the extraction force exerted

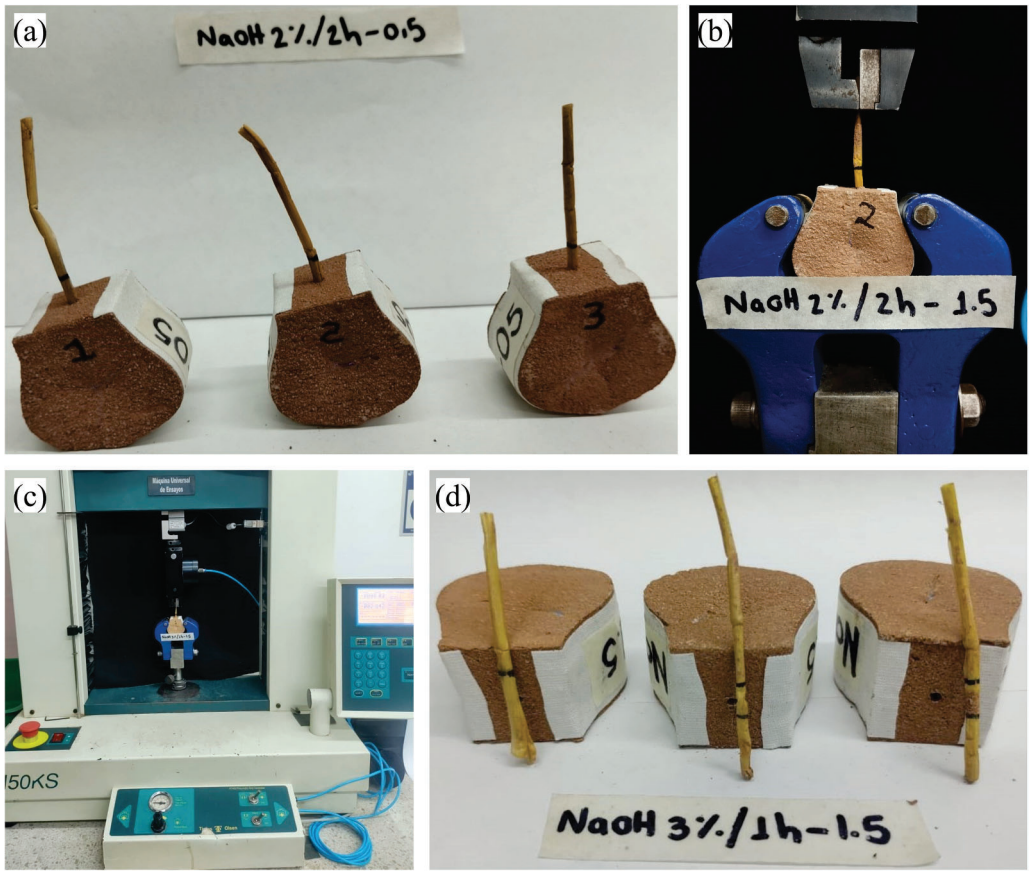

Fig. 6. Single-fiber pullout test process. (a) Specimens before the test, (b) Specimen assembly, (c) Test run, (d) Specimens with fibers pulled out.

and the area of the embedded fiber. The bond stress (τ) was calculated using Eq. (1). The Eq. (1) identified the force required to detach the fiber from the matrix [43].

$$\tau = \frac{F_{max}}{A_{emb}} \quad (1)$$

Where:

F_{max} = Maximum fiber pullout force

A_{emb} = Fiber surface embedded in the matrix

The A_{emb} was calculated using Eq. (2). Calculation necessary to determine the τ

$$A_{emb} = Perimeter * E - length \quad (2)$$

Using the results in Table 4, the data in Eq. (2) and Eq. (1) were replaced to determine the τ for RSS-3W/ut-0.5:

$$A_{emb} = 8.13\ mm * 5\ mm \quad (3)$$

$$\tau = \frac{1.70\ N}{40.65\ mm^2} \quad (4)$$

The calculations of Eqs. (3) and (4) were performed to determine the τ of the other fibers.

Tables 4, 5, and 6 present the averaged results of the single-fiber pullout test performed on the samples. The tables show the Sample-I. The perimeter of the embedded rice straw. The E-length. The A_{emb}. The maximum extraction force of the fiber (F_{max}). The τ.

The single-fiber pullout test identified that the rice straw fibers embedded 5 mm, 10 mm, and 15 mm showed total detachment from the matrix. The reason why the τ results were low. This phenomenon was generated due to the small area of fiber-matrix interaction. However, this fiber detachment favors the semi-ductile behavior of the Green composite to be produced due to the increased energy absorption capacity per cracked area. A phenomenon that is evident after the fracture of the matrix. At this point the fibers with shorter embedded lengths allow their detachment generating post-fracture friction of the matrix.

In contrast, if a Green composite with higher energy absorption capacity before matrix failure is to be produced, higher adhesion can be promoted by increasing the embedded fiber length. Increasing gradually until an increase in pullout force is achieved to the point of causing fiber breakage failure. At this point, the crack propagation force exceeds the tensile strength of the fiber causing it to break. The above, considering the intended application of the Green composite where fiber detachment or breakage under tensile forces is preferred.

However, it must be considered that in addition to the embedded area of the vegetable fiber, the fiber-clay matrix adhesion phenomena are important for the τ. Phenomenon in which roughness in the surface topography is an important feature to ensure opposition to detachment and increased frictional forces.

3.2. Individual fiber behavior

In the single-fiber pullout test carried out on rice straws embedded in a clay matrix, it can be considered that of the 5 possible causes that generate friction effects when pulled out of the matrix, roughness can be controlled by physical or chemical treatments before their implementation as reinforcement fibers. Other possible causes can be controlled at the time of pouring the mixture into the mold or simply by stabilization of the clay matrix. The above, knowing the final yield of the green composite to be produced.

Table 4
Results single-fiber pullout test samples with 5 mm of embedded fiber.

Sample	(mm)		A_{emb} (mm^2)	F_{max} (N)	τ (MPa)
	Perimeter	E-length			
RSS-3W/ut-0.5	8.13	5	40.65	1.70	0.041
NaOH 1 %/1h-0–5	7.53		37.65	3.67	0.097
NaOH 2 %/2h-0.5	7.73		38.65	7.17	0.185
NaOH 3 %/1h-0.5	7.67		38.35	4.83	0.125

Table 5
Results single-fiber pullout test samples with 10 mm of embedded fiber.

Sample	(mm)		A_{emb} (mm^2)	F_{max} (N)	τ (MPa)
	Perimeter	E-length			
RSS-3W/ut-1	7.48	10	74.8	3.57	0.047
NaOH 1 %/1h-1	7.44		74.4	20.48	0.275
NaOH 2 %/2h-1	6.77		67.7	6	0.088
NaOH 3 %/1h-1	7.03		70.3	9.07	0.129

Table 6
Results single-fiber pullout test samples with 15 mm of embedded fiber.

Sample	(mm)		A_{emb} (mm^2)	F_{max} (N)	τ (MPa)
	Perimeter	E-length			
RSS-3W/ut-1.5	7.34	15	110.1	4.30	0.039
NaOH 1 %/1h-1.5	7.85		117.75	7.30	0.061
NaOH 2 %/2h-1.5	7.56		113.4	10	0.088
NaOH 3 %/1h-1.5	7.89		118.35	5.57	0.047

Fig. 7 shows the diagram of the single-fiber pullout test. The figure shows the initial tensile force (Itf) exerted in the test. The ultimate tensile force (Utf) that determines the debonding from the matrix is shown. The tensile force released (Tfr) due to fiber detachment is shown. The initial friction force (Iff) is shown, which identifies the fiber's opposition to displacement. The Ultimate friction force (Uff) is shown which indicates the friction loss between the fiber and the matrix. The primary friction zone (Pfz) resulting from the initial process of fiber detachment from the matrix due to Poisson's shrinkage phenomenon is shown. The friction length (Flh) route by the fiber is shown. The moment when the fiber is removed (Rfr) from the matrix is shown.

Figs. 8, 9, and 10 show the individual fiber behavior in the single-fiber pullout test. For a better view of the results, only the representative curves that were close to the average data are presented for each fiber series.

Fig. 8 shows graphically the behavior of the 5 mm embedded fibers at the time of extraction. Fig. 8a shows the low force required for the detachment of the RSS 3W/ut-0.5 fibers at 1.7 N. Minimal strength attributed to low fiber-matrix interaction due to lack of chemical treatment. The not-so-considerable force required to extract NaOH 1

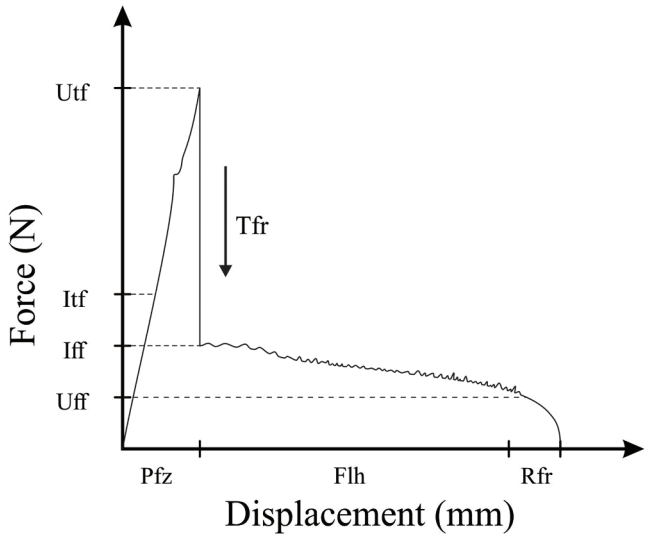

Fig. 7. Single-fiber pullout test diagram.

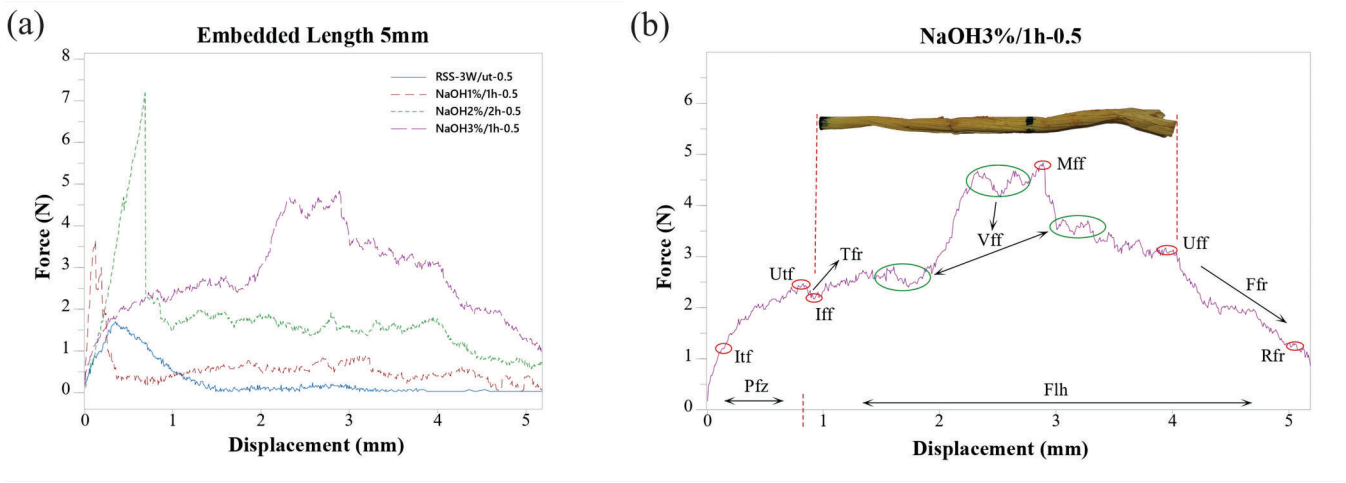

Fig. 8. Force-displacement graph embedded fiber 5 mm.

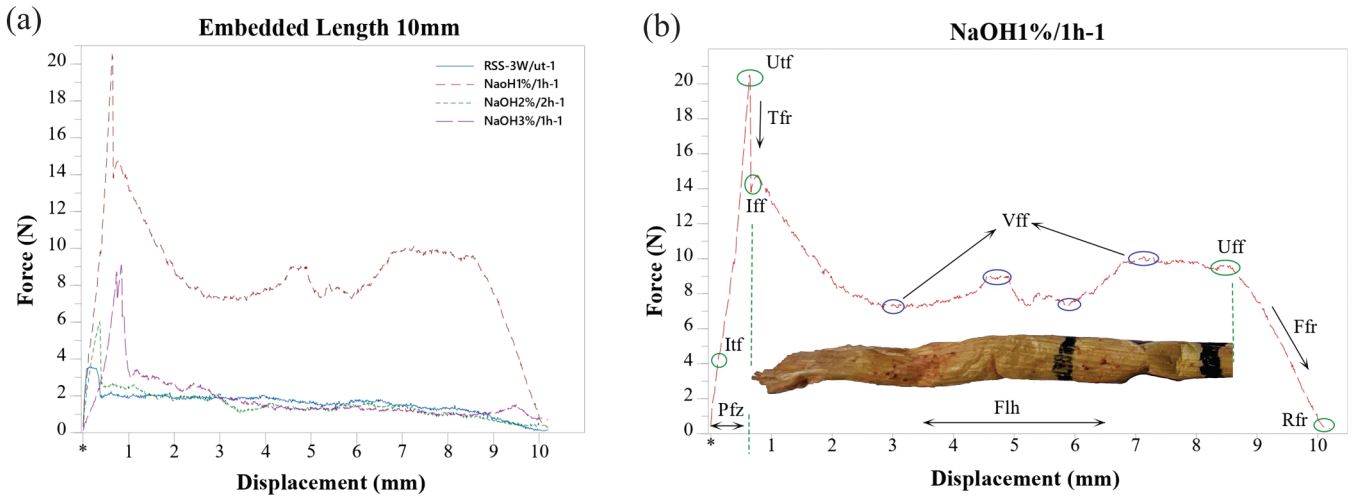

Fig. 9. Force-displacement graph embedded fiber 10 mm.

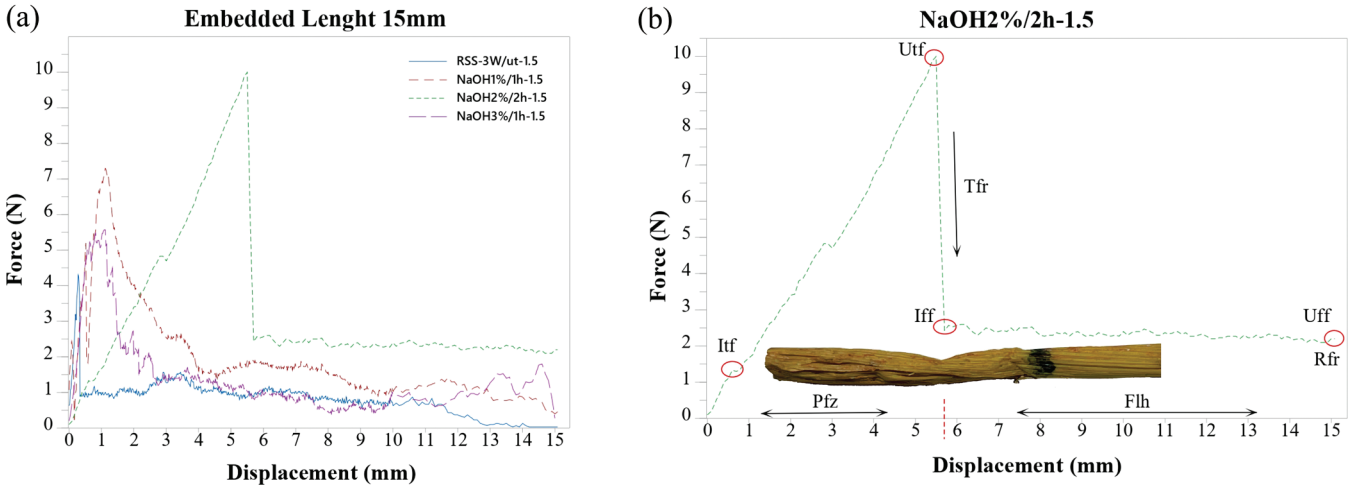

Fig. 10. Force-displacement graph embedded fiber 15 mm.

%/1h-0.5 with 3.67 N is shown. Medium strength which can be attributed to the short length of embedded fiber. These 2 fibers also showed minimal frictional resistance before their removal from the matrix. The pull-out resistance of NaOH 2 %/2h-0.5 is shown for which 7.17 N is the highest value among the extracted fibers. This resistance was caused by the roughness in the surface topography of the fiber due to the chemical

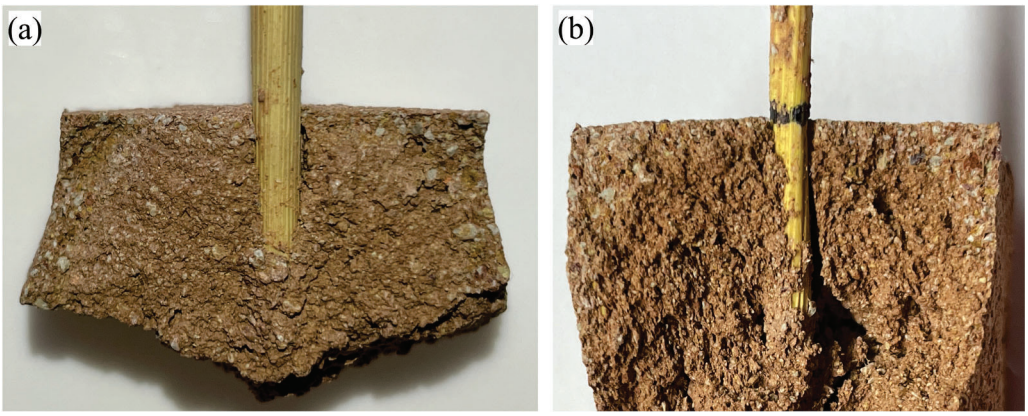

Fig. 11. Fiber-matrix interaction. (a) Untreated fiber-clay matrix interaction, (b) Mercerized fiber-clay matrix interaction.

treatment. Characteristic that caused adhesion between the fiber and the matrix generating opposition to frictional forces (see Fig. 11b). In the study carried out by Pearson et al. [44] on high-density polyethylene fibers. The authors indicated that after the separation of the fiber from the matrix, there is a considerable drop in the extraction force resulting in slow fiber removal due to the friction exerted. Strength decreases in parallel with the reduction of the embedded area of the fiber.

Fig. 8b depicts the phenomenon of the NaOH 3 %/1h-0.5. The graph describes the forces that were described in the single-fiber pullout test diagram (see Fig. 7). The phenomenon corresponding to the maximum friction force (Mff) is shown. Force that can be generated due to the extra friction caused by the surface roughness caused by the alkaline treatment and the geometrical irregularity of the vegetable fibers due to their natural origin (see Fig. 3d and Fig. 12). This phenomenon of increased extraction force was described by the authors Zhang et al. [45]. The researchers determined the bonding properties of the polyvinyl alcohol fiber interface in alkali-activated slag/fly ash mixtures. In the research, the authors indicated that after fiber detachment a displacement stiffening effect was generated which increased the pull-out resistance.

Fig. 8b also shows the phenomenon of variation in friction force (Vff) due to friction phenomena (see Fig. 3). The graph indicates the phenomenon corresponding to the friction force released (Ffr) where the fiber ceases to resist pullout force (see Fig. 7). The graph identifies the length route in the Pfz. This length is very close to the % elongation obtained by the fiber in the tension and elongation test (see Table 1).

Pfz is the result of the initial process of fiber detachment with the matrix. This phenomenon is related to Poisson contraction. In the primary friction zone, the fiber diameter shrinks due to elongation caused by the applied extraction force. Consequently, the shrinkage generated in the fiber cross-section causes a short primary friction zone during the shedding process. This length is less than the friction length that is generated before the total removal of the fiber. The % elongation of the fiber significantly influences the shrinkage of its cross-section. Characteristic for determining fiber displacement at Pfz and Flh.

Fig. 9 shows the behavior of the embedded fibers at 10 mm at the time of extraction. Fig. 9a shows the minimum force exerted to detach the RSS-3W/ut-1 with 3.57 N. Extraction force that doubled the force generated in the 5 mm extraction simply by increasing the length of the embedded fiber (see Fig. 8). This fiber has minimal adhesion between components. Characteristic attributed to the lack of roughness in its surface topography (See Fig. 11a). Shown is the extraction strength of NaOH 2 %/2h-1 with 6 N. Force less than described by 5 mm. A phenomenon occurred due to fiber stiffness due to the removal of lignin and hemicellulose by chemical treatment [46]. A characteristic that avoids the reduction of the fiber diameter at the moment of shrinkage due to the drying of the matrix, reducing anchorage zones and avoiding friction forces (see Fig. 3). NaOH 3 %/1h-1 required a force of 9.07 N to achieve detachment with the matrix. This force was generated due to the adhesion of the matrix to the roughened areas on the fiber Surface (see Fig. 11b). Roughness is caused by the removal of key polymers and impurities due to the mercerization process [20]. NaOH 1 %/1h-1 had the highest release force at 20.48 N. This fiber also exhibited the Vff phenomena in its friction length.

Fig. 9b shows the phenomenon occurring in the NaOH 1 %/1h-1. Initially, the fiber showed an almost linear behavior until it reached the maximum force that generated its extraction. Force is caused by roughness in its surface topography due to chemical treatment. This roughness allowed the matrix to adhere to the fiber causing opposition

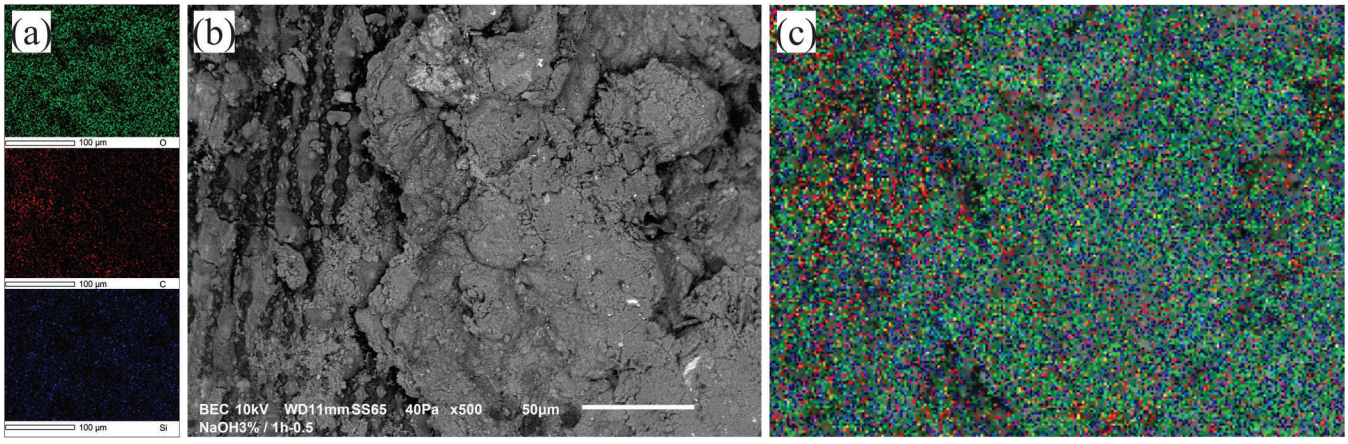

Fig. 12. Description of the phenomena occurring in NaOH 3 %/1h-0.5. (a) Elemental chemical colour code, (b) Matrix-fiber interaction, (c) EDS mapping.

to its detachment (see Fig. 11b).

After 20.48 N the extraction strength of NaOH 1 %/1h-1 decreased considerably due to fiber detachment (see Fig. 7). However, the fiber showed opposition to displacement due to frictional forces caused by the pressure exerted in drying shrinkage (see Fig. 12). Phenomenon causing geometrical irregularities in the fiber due to its flexibility (see Fig. 13). The same phenomenon was described by the research carried out by Park et al. [47]. In their research, the authors analyzed the pullout behavior of metallic fibers in concrete mixes. In the research, the authors concluded that the geometric shapes of the fibers directly influence their tensile strength.

Fig. 10 shows the behavior of 15 mm embedded fibers under extraction force. Fig. 10a shows the extraction force achieved by the RSS-3W/ut-1.5 with 4.30 N. Minimal strength is required due to a lack of adhesion between fiber and matrix (see Fig. 11a). A phenomenon that is still evident due to the lack of any kind of mechanical or chemical treatment to improve its surface topography. The pullout force that allowed the detachment of the NaOH 3 %/1h-1.5 with 5.57 N is shown. Force lower than reported in the force-displacement graph of the embedded fibers 10 mm (see Fig. 9). Phenomenon may be caused by the small geometrical irregularity of the fiber. The force required to detach the NaOH 1 %/1h-1.5 fiber with 7.30 N is shown. Force reduced by >50 % compared to the extraction force of 10 mm embedded fiber (see Fig. 9). This atypical phenomenon can be attributed to positive changes in the geometric irregularity of the fiber due to drying shrinkage. Phenomenon that could correct irregularities by lateral forces exerted (see Fig. 3c). The influence of the geometrical modification of the fiber on its opposition to tensile forces was described by the research carried out by the authors Lin et al. [48]. The researchers conclude that fiber shape, fiber diameter, embedded angle, embedded length, and surface roughness are physical characteristics involved in fiber behavior under extraction forces. It shows the phenomenon that occurred in NaOH 2 %/2h-1.5.

Fig. 10b shows the behavior of NaOH 2 %/2h-1.5 at the 10 N required for detachment. The considerable route is shown in the Pfz. This route was generated due to the rupture of the cellulose fibrils which increased their elongation % (see Table 1 and Fig. 13, Fig. 14). The friction force exerted did not show any variability in its route due to the regular geometry of the fiber. A similar phenomenon was concluded by the authors Rezaie et al. [49]. In their research, the authors used polyethylene fibers with polydopamine in cementitious matrixes. The authors indicated that after fiber extraction a linear friction extraction behavior was generated due to the regularity of the surface roughness. In the extraction process, there is initially an upward momentum of the curve that reaches the maximum exerted force that detaches the fiber Utf. The outside is then released due to the detachment Tfr. This is followed by the friction phenomenon that resists the complete removal of the fiber from the matrix Flh (see Fig. 7) [45,50].

3.3. Vegetal fiber-clay matrix adhesion phenomenon

The average force-displacement curves allowed the analysis of the interfacial behavior of rice straw fibers embedded at 50 % of their working length. The graphs show the resistance to pullout that the fiber initially opposes. However, at the moment of detachment there is a considerable decrease in the extraction force due to the loss of fiber-matrix interaction (see Fig. 7). After the detachment of the fiber, the friction phenomenon occurs. Depending on the physical characteristics of the fiber, this phenomenon may require higher forces than those exerted during the initial detachment, thus achieving the Mff (see Fig. 3). Opposition to friction is one of the characteristics of vegetable fibers due to irregularities in their surface topography. These geometric irregularities are typical of vegetable fibers or can be caused by mercerization processes [48].

The alkaline treatment increases the roughness of the surface topography of the vegetable fibers, ensuring better adhesion to the matrix (see Fig. 11b). Characteristic causing opposition to displacement by friction phenomena. However, the NaOH concentration and the exposure time of the fiber in the alkaline solution must be controlled to avoid damage that compromises the mechanical behavior of the vegetable fibers [51].

Fig. 11 shows the fiber-matrix interaction generated inside the sample. Fig. 11a shows the poor adhesion of clay matrix particles in the RSS-3W/ut. The effect generated by the lack of some kind of treatment generates roughness in its surface topography [52]. The regular and smooth surface of RSS 3W/ut prevents interfacial bonding with the matrix. This effect reduces its resistance to pullout forces.

Fig. 11b shows the clay matrix adhesion of the chemically treated fibers. This adhesion allows the fiber to be coated by the matrix, generating mechanical anchorage on its surface. Feature that considerably increases its resistance to tensile forces. The mercerization process causes the anchoring of matrix particles in the rough areas of the fiber, generating a positive interaction that increases its resistance to external forces [53].

3.4. SEM observations and EDS mapping

3.4.1. Longitudinal observation

The SEM observations made it possible to contextualize the bonding phenomena between the RSS and the clay matrix. EDS mapping allowed the identification of the elemental chemistry present on the surface of the fibers and helped in the interpretation of the SEM observations.

Fig. 12 shows the SEM observation and EDS mapping performed on the NaOH 3 %/1 h 0.5. Fig. 12a shows the colour identification of the EDS mapping. The green colour represents Oxygen. Red colour represents Carbon. Blue colour represents Silica. Fig. 12b shows the adhesion of the matrix due to the roughness of the fiber surface topography caused by the alkaline treatment. The roughness and surface irregularity

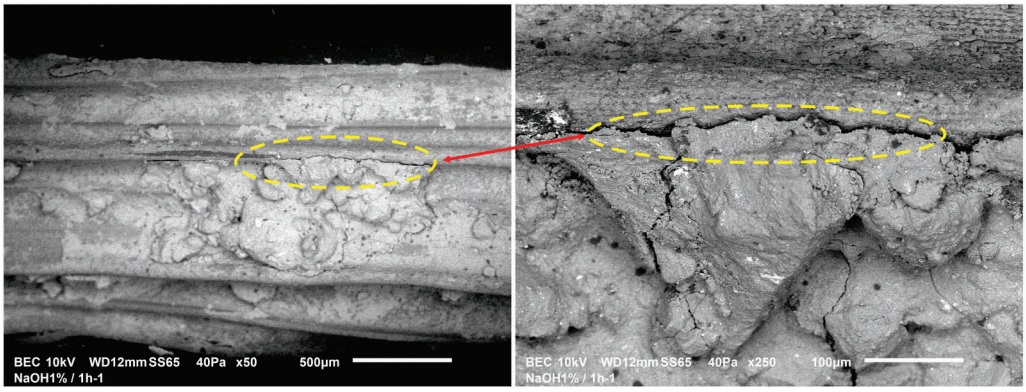

Fig. 13. Adhesion phenomenon clay matrix-fiber NaOH 1 %−1h-1.

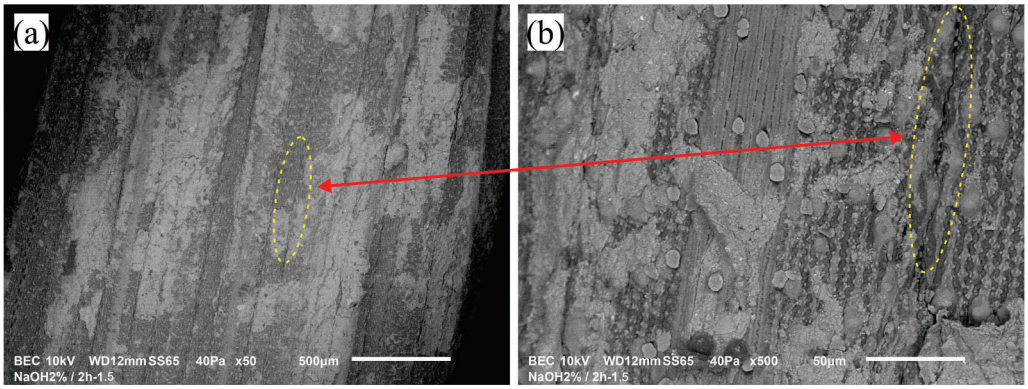

Fig. 14. Pullout behavior of the NaOH 2 %/2h-1.5. (a) Geometric regularity, (b) Fibril breakage.

of the plant fibers increase the friction forces after their detachment from the matrix. Characteristic describing the phenomenon occurring in the fiber at the moment of its extraction (see Fig. 8b). Fig. 12c shows the chemical dispersion generated by EDS mapping. It shows the poor visualization of the carbon element that makes up the cellulose fibers due to the surface coating generated by the matrix. Silica and oxygen are dispersed due to their presence in the matrix.

Fig. 13 shows the adhesion phenomenon of the matrix on the NaOH 1 %−1h-1 fiber. The figure shows the irregularity in the surface topography of the fiber that favors interaction with the matrix. The mechanical anchoring by confinement effect is shown (see Fig. 3c). The phenomenon occurs due to drying shrinkage of the matrix exerting pressure on the fiber surface. The pressure exerted by drying shrinkage causes surface deformation in the fiber, generating anchorage zones. These deformations are attributed to the flexibility of the fiber due to the presence of lignin and hemicellulose that were not removed by the alkaline treatment at lower concentrations and short exposure time. The anchorage favors fiber-matrix interaction, requiring higher forces for detachment and higher friction in the displacement at the moment of total removal of the matrix [54]. A similar phenomenon was concluded by the authors Alioui et al. [55]. In their research, the authors included wheat straw in mixtures with clay matrix for earth brick production. The authors concluded that straw provides self-stabilization of the clay matrix due to its fibrous structure composed of cellulose. This type of stabilization is related to the deformation capacity of the fibers under external forces.

Fig. 14 shows the phenomenon occurring in the NaOH 2 %/2h-1.5. Fig. 14a shows the geometrical regularity of the fiber due to its opposition to deformation. Geometric regularity is caused by the rigidity caused by the removal of lignin and hemicellulose. The fiber has surface interaction with the matrix. A characteristic that allows anchorage with the matrix, preventing its detachment. Fig. 14b shows the surface breakage caused by extraction forces. The fibril breakage favors fiber elongation. The percentage of elongation increases the fiber's opposition to its detachment from the matrix.

Fig. 15 shows the influence of alkaline treatment on the generation of anchor pores. Fig. 15a shows the EDS mapping showing the silica bodies present in the non-functional stomata. Fig. 15b shows obstruction of non-functional stomata by silica bodies. Fig. 15c shows the removal of the silica bodies as an effect of the alkaline treatment generating pores that allow the matrix to enter. A phenomenon that generates anchorage zones favoring fiber-matrix interaction. A similar conclusion was made by authors Gholampour & Ozbakkaloglu [56]. In their review article, the authors concluded that the presence of silica bodies, wax, and impurities on the surface of the vegetable fibers prevents anchorage with the matrix. A phenomenon leading to the low mechanical performance of Green composites.

3.4.2. *Cross-sectional observation*

Fig. 16 shows the cross-sectional observation of the embedded fibers. This observation made it possible to determine the perimeter of each of the fibers to calculate τ (see Tables 4, 5, and 6). Observation identified the phenomenon of adhesion in the cross-sectional area of the vegetable fibers due to the vascular bundles that make up the conductive tissue [20]. Fig. 16a shows the xylem and phloem, the main elements of the vegetable fiber conducting tissue. The inner diameter of the rice straw is also shown. Fig. 16b shows the cross-section of the RSS-3W/ut-1. Fig. 16c shows the cross-section of the NaOH 1 %/1h-1. Fig. 16d shows the cross-section of the NaOH 2 %/2h-1. Fig. 16e shows the cross-section of the NaOH 3 %/1h-1. The figures show the ingress of the clay matrix into the inner diameter and porous tissue of the xylem and phloem. Phenomenon causing fiber-matrix interaction in the cross-sectional area of vegetable fibers. This phenomenon adds up to efforts to oppose detachment when removing the fiber from the matrix. This special characteristic of vegetable fibers favors the fiber-matrix interaction in its longitudinal and transversal area, increasing its resistance to tensile forces and improving the mechanical properties of the Green Composite.

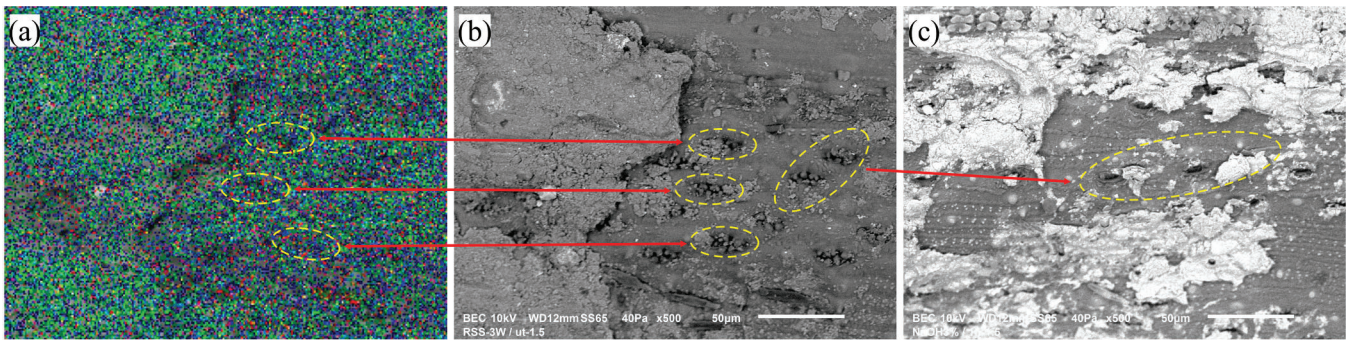

Fig. 15. Influence of NaOH on pores generation. (a) EDS mapping, (b) Silica bodies in non-functional stomata, (c) Anchoring pores.

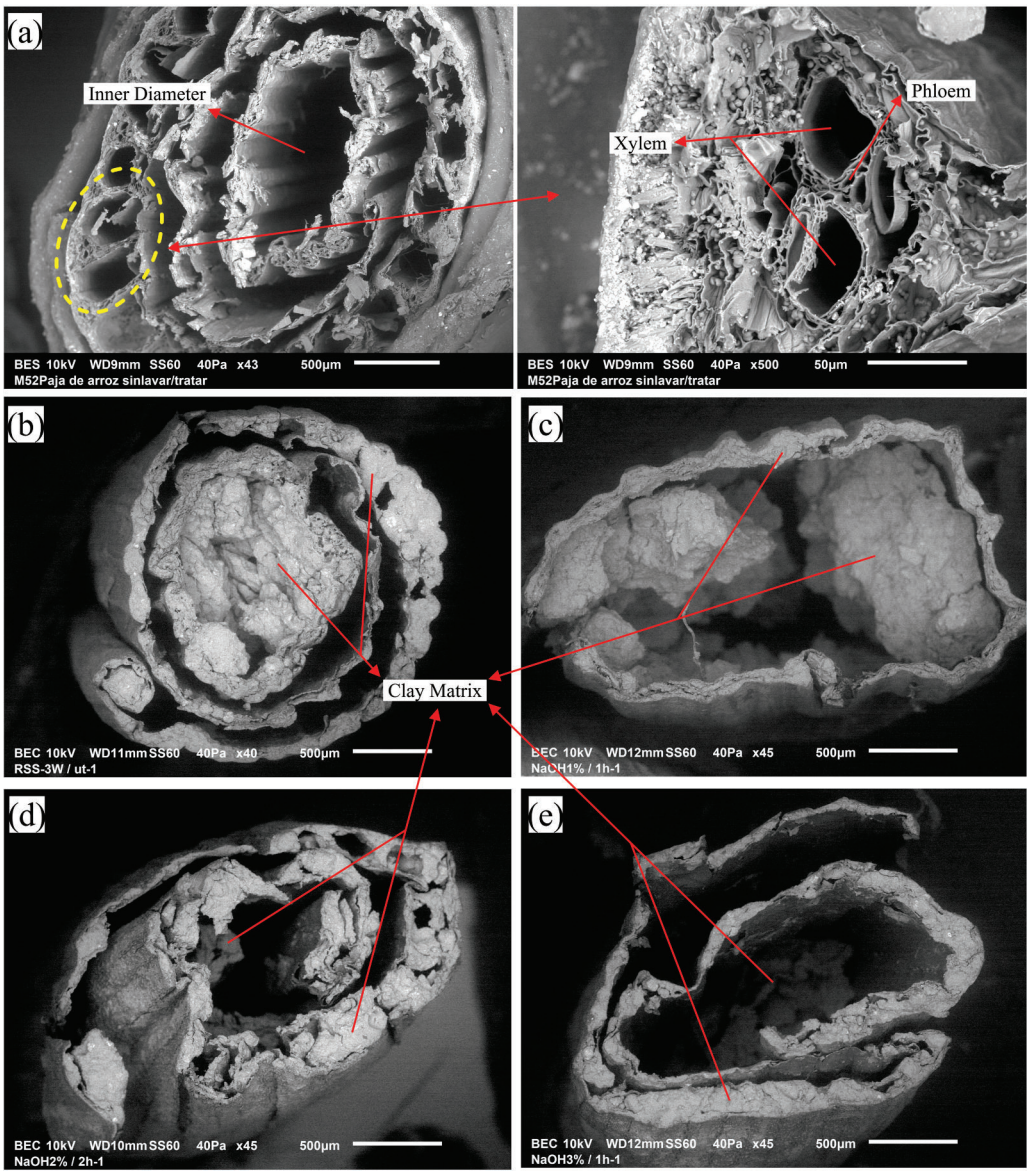

Fig. 16. Observation SEM cross-section. (a) Conducting tissue, (b) RSS-3W/ut-1, (c) NaOH 1 %/1h-1, (d) NaOH 2 %2h-1, (e) NaOH 3 %/1h-1.

4. Conclusions

In general, it is concluded that the single-fiber pullout test is an efficient method to determine the physical characteristics and the embedding length of vegetable fibers intended to be used as a reinforcement element in the production of Green composites. The results identify the influence of the surface topography of the vegetable fibers on their pullout behavior. This phenomenon makes it possible to predict the mechanical behavior of the Green composite under tensile forces.

The implementation of the single-fiber pullout test avoids the excessive production of specimens for destructive tests to determine the mechanical behavior of the experimental mixtures. As a result, the single-fiber pullout test helps research by reducing execution time and budget.

In particular, through the analysis of the results obtained in the present investigation, the following conclusions were reached:

- Rice straw fibers embedded 5 mm, 10 mm, and 15 mm show detachments with the matrix due to low bonding stress results. This phenomenon favors the semi-ductile behavior of the green composites to be produced. This feature prevents the detachment of particles by fracture of the material.
- To produce a Green composite with a higher post-fracture energy absorption capacity of the matrix, a higher fiber-matrix interaction must be promoted by gradually increasing the embedded fiber length.
- The rice straw has a non-constant cross-section due to deformations or irregularities. For this reason, there were physical obstructions when the fiber was extracted. This type of obstruction generates a positive increase in fiber-matrix adhesion.
- The natural origin and the difference in diameters of the rice straw influenced its behavior under detachment forces with the matrix.
- The stiffness of the rice straw due to an alkaline treatment in NaOH concentrations of 2 % and 2 h of exposure prevented the confinement of the fiber by drying shrinkage of the clay matrix. This phenomenon facilitated its extraction by generating minimum opposition to friction.
- The % elongation of the rice straw fibers favored the requirement of the initial detachment force. However, the elongation can be unfavorable at the moment of displacement for its extraction from the

matrix. This phenomenon is attributed to the low friction caused by Poisson's shrinkage phenomenon.

- The loss of volume and shrinkage due to drying of the clay mixture must be taken into consideration when making the molds for the single-fiber pullout test. This is due to the normative dimensions of the specimens to be clamped by the grips.
- The best-performing alkaline treatment was NaOH 1 %1 h. The optimum length of the embedded rice straw fiber was 10 mm which corresponds to a working length of 20 mm for the production of Green composites. However, this conclusion cannot be generalized due to the vegetable origin of the rice straw and the mercerization process to which it was exposed. These characteristics present determining variables depending on the geographical area where the crop is located, the climatic characteristics, the cultivation process, the harvesting process, and the irrigation system, among other factors corresponding to the sowing of the cereal where the straw is to be harvested. For this reason, the fiber-matrix interaction of any vegetable fiber intended to be used as a reinforcement element in clay matrices must be analyzed individually based on the processes carried out in this research.

CRediT authorship contribution statement

Oswaldo Hurtado-Figueroa: Writing – original draft, Validation, Resources, Methodology, Investigation, Formal analysis, Data curation, Conceptualization. **Humberto Varum:** Writing – review & editing, Supervision, Methodology, Formal analysis. **María Isabel Prieto:** Writing – review & editing, Supervision, Data curation. **Romel J Gallardo Amaya:** Writing – review & editing, Supervision, Data curation. **Alfonso Cobo Escamilla:** Writing – review & editing, Supervision, Methodology, Formal analysis.

Declaration of competing interest

The authors declare that they have no known competing financial interests or personal relationships that could have appeared to influence the work reported in this paper.

Funding

This research received no external funding.

Acknowledgement

The authors are grateful for the laboratories; Laboratorio de Análisis de Materiales para la Construcción LABMAC—SENA—Centro C.I.E.S Regional Norte de Santander. Laboratorio de Biotecnología y Nanotecnología —Tecnoparque SENA— Nodo—Cúcuta. Laboratorio de Servicios Tecnológicos del Centro de Manufactura en Textil y Cuero - SENA—Bogotá. Laboratorio de Caracterización del Grupo Materiales Compuestos de la Universidad del Valle.

Data availability

Data will be made available on request.

References

[1] O. Hurtado-Figueroa, E.J. Vega-Vanegas, J.A. Cárdenas-Gutiérrez, Mechanical strength of experimental mortars for plastering with partial addition of fly ash and hydrated lime, J. Phys.: Conf. Ser. 1386 (2019) 012071. https://iopscience.iop.org/article/10.1088/1742-6596/1386/1/012071.

[2] S. Karthik, P. Karunakaran, G. Velmurugan, Experimental investigation of WE43 (T6) magnesium metal matrix composites to enhance mechanical properties and EDM process parameters, Int. J. Electrochem. Sci 19 (2024), https://doi.org/10.1016/j.ijoes.2024.100553.

[3] S. Adil, B. Kumar, P.S. Panicker, D.H. Pham, J. Kim, High-performance green composites made by cellulose long filament-reinforced vanillin epoxy resin, Polym. Test 123 (2023) 108042, https://doi.org/10.1016/j.polymertesting.2023.108042.

[4] B. Fei, H. Yang, J. Yang, D. Wang, H. Guo, H.Hou. Fei, et al., Sustainable compression-molded bamboo fibers/poly (lactic acid) green composites with excellent UV shielding performance, J. Mater. Sci. Technol. 205 (2024) 247–257, https://doi.org/10.1016/j.jmst.2024.03.074.

[5] S.C. Das, A.D. La Rosa, S. Goutianos, S. Grammatikos, Effect of accelerated weathering on the performance of natural fibre reinforced recyclable polymer composites and comparison with conventional composites, Compos. C Open Access 12 (2023) 100378, https://doi.org/10.1016/j.jcomc.2023.100378.

[6] M. Raquibul, I.J. Davies, A. Pramanik, M. John, K. Biswas, Potential of recycled PLA in 3D printing: a review, Sustain. Manuf. v. Econ. 3 (2024) 100020, https://doi.org/10.1016/j.smse.2024.100020.

[7] A.N. Shankar, A.N. Netravali, R.A. Mensah, O. Das, Composites Part C: open Access Microscale combustion calorimetry assessment of green composites made with chicken feather-modified soy protein resins and jute fabric, Compos. C Open Access 12 (2023) 100394, https://doi.org/10.1016/j.jcomc.2023.100394.

[8] O. Hurtado-Figueroa, J.P.R. Suárez, J.A. Cárdenas-Gutiérrez, Subgrade improvement by the replacement of conventional stone aggregate by biosanitary waste treated, J. Phys.: Conf. Ser. 1329 (2019) 012010. https://iopscience.iop.org/article/10.1088/1742-6596/1329/1/012010.

[9] M. Gomaa, S. Schade, D.W. Bao, Y.M. Xie, Automation in rammed earth construction for industry 4.0: precedent work, current progress and future prospect, J. Clean. Prod. 398 (2023) 136569, https://doi.org/10.1016/j.jclepro.2023.136569.

[10] M. Valenzuela, G. Ciudad, J.P. Cardenas, C. Medina, A. Salas, A. Oñate, et al., Towards the development of performance-efficient compressed earth blocks from industrial and agro-industrial by-products, Renew. Sustain. Energy Rev. 194 (2024) 114323, https://doi.org/10.1016/j.rser.2024.114323.

[11] C. Canditone, L. Diana, A. Formisano, H. Rodrigues, R. Vicente, Failure mechanisms and behaviour of adobe masonry buildings: a case study, Eng. Fail. Anal. 150 (2023) 107343, https://doi.org/10.1016/j.engfailanal.2023.107343.

[12] K. Agyekum, E. Kissi, J.C. Danku, Professionals' views of vernacular building materials and techniques for green building delivery in Ghana, Sci. Afr. 8 (2020) e00424, https://doi.org/10.1016/j.sciaf.2020.e00424.

[13] E. Hamard, C. Cammas, B. Lemercier, B. Cazacliu, J.C. Morel, Micromorphological description of vernacular cob process and comparison with rammed earth, Front. Archit. Res. 9 (2020), https://doi.org/10.1016/j.foar.2019.06.007, 203e215.

[14] O. Hurtado-Figueroa, H. Varum, M.I. Prieto, R.J. Gallardo, A.C. Escamilla, The alkaline treatment and its influence on the physicomechanical properties of plantain pseudostem fibers - A comparative study of treated and untreated fibers, Heliyon. 11 (2025) e41843, https://doi.org/10.1016/j.heliyon.2025.e41843.

[15] H. Elmoudnia, P. Faria, R. Jalal, M. Waqif, L. Saadi, Effectiveness of alkaline and hydrothermal treatments on cellulosic fibers extracted from the Moroccan Pennisetum Alopecuroides plant: chemical and morphological characterization, Carbohydr. Polym. Technol. Appl. 5 (2023) 100276, https://doi.org/10.1016/j.carpta.2022.100276.

[16] P. Pandiarajan, M. Kathiresan, P.G. Baskaran, J. Kanth, Characterization of raw and alkali treated new cellulosic fiber from the rinds of Thespesia populnea plant, J. Nat. Fibers (2020) 1–12, https://doi.org/10.1080/15440478.2020.1852996.

[17] A. Hasan, M.S. Rabbi, M.M. Billah, M.A. Hasib, Effect of chemical treatments on properties of injection molded Nypa fruticans fiber reinforced polypropylene composite, Heliyon 8 (2022) e11967, https://doi.org/10.1016/j.heliyon.2022.e11967.

[18] P. Valasek, M. Müller, V. Sleger, V. Kolar, M. Hromosava, R. Amato, et al., Influence of Alkali treatment on the microstructure and mechanical properties of Coir and Abaca fibers, Mater. (Basel) 14 (2021) 2636, https://doi.org/10.3390/ma14102636.

[19] R.D. Murwamadala, L.B. Mathebela, M.P. Mubiayi, Impact of Alkali treatment on the internal microstructure, surface topography and the resulting mechanical properties of single sisal, J. Nat. Fibers 21 (2024) 2370028, https://doi.org/10.1080/15440478.2024.2370028.

[20] O. Hurtado-Figueroa, A.C. Escamilla, H. Varum, The mercerization process and its impact on rice straw surface topography, Buildings 13 (2023) 1–29, https://doi.org/10.3390/buildings13071573.

[21] T.T. Stanislas, J.F. Tendo, R.S. Teixeira, E.B. Ojo, G.C. Komadja, M. Kadivar, et al., Effect of cellulose pulp fibres on the physical, mechanical, and thermal performance of extruded earth-based materials, J. Build. Eng. 39 (2021) 102259, https://doi.org/10.1016/j.jobe.2021.102259.

[22] C. Babéa, D.K. Kidmoa, A. Tomb, R.R.N. Mvondoc, R.B.E. Boumd, N. Djongyanga, Thermomechanical characterization and durability of adobes reinforced with millet waste fibers (sorghum bicolor), Case Stud. Constr. Mater. 13 (2020) e00422, https://doi.org/10.1016/j.cscm.2020.e00422.

[23] E.B. Ojo, K.O. Bello, K. Mustapha, R.S. Teixeira, S.F. Santos, H. Savastano, Effects of fibre reinforcements on properties of extruded alkali activated earthen building materials, Constr. Build. Mater. 227 (2019) 116778, https://doi.org/10.1016/j.conbuildmat.2019.116778.

[24] G. Araya-Letelier, F.C. Antico, C. Burbano-Garcia, J. Concha-Riedel, J. Norambuena-Contreras, J. Concha, et al., Experimental evaluation of adobe mixtures reinforced with jute fibers, Constr. Build. Mater. 276 (2021) 122127, https://doi.org/10.1016/j.conbuildmat.2020.122127.

[25] K. AlShuhail, A. Aldawoud, J. Syarif, I.A. Abdoun, Enhancing the performance of compressed soil bricks with natural additives: wood chips and date palm fibers, Constr. Build. Mater. 295 (2021) 123611, https://doi.org/10.1016/j.conbuildmat.2021.123611.

[26] M.M. Salih, A.I. Osofero, M.S. Imbabi, Constitutive models for fibre reinforced soil bricks, Constr. Build. Mater. 240 (2020) 117806, https://doi.org/10.1016/j.conbuildmat.2019.117806.
[27] F.F. Khorasani, M.Z. Kabir, Experimental study on the effectiveness of short fiber reinforced clay mortars and plasters on the mechanical behavior of adobe masonry walls, Case Stud, Constr. Mater. 16 (2022) e00918, https://doi.org/10.1016/j.cscm.2022.e00918.
[28] F. Ávila, E. Puertas, R. Gallego, Characterization of the mechanical and physical properties of stabilized rammed earth : a review, Constr. Build. Mater. 325 (2022) 126693, https://doi.org/10.1016/j.conbuildmat.2022.126693.
[29] V.C. Li, C. Wu, S. Wang, A. Ogawa, T. Saito, Interface tailoring for strain-hardening polyvinyl alcohol- engineered cementitious composite (PVA-ECC), ACI Mater. J. 99 (2002) 463–472. https://www.researchgate.net/publication/279938212_Interface_tailoring_for_strainhardening_polyvinyl_alcohol-engineered_cementitious_composite_PVA-ECC.
[30] Y. Deng, Z. Zhang, C. Shi, Z. Wu, C. Zhang, Steel Fiber – Matrix interfacial bond in Ultra-high performance concrete : a review, Engineering 22 (2023) 215–232, https://doi.org/10.1016/j.eng.2021.11.019.
[31] K. Lou, P. Xiao, G.P. Ong, B. Li, A. Kang, Z. Wu, Micromechanical behavior of single fiber-asphalt mastic interface: experimental studies by self-designed innovative pullout test, Constr. Build. Mater 414 (2024) 134873, https://doi.org/10.1016/j.conbuildmat.2024.134873.
[32] V.P. Dang, D.J. Kim, Rate-sensitive pullout resistance of smooth-steel fibers embedded in ultra-high-performance concrete containing nanoparticles, Cem. Concr. Compos. 140 (2023) 105109, https://doi.org/10.1016/j.cemconcomp.2023.105109.
[33] A. Antonova, M. Eik, J. Puttonen, Importance of the surface roughness of a steel fibre pulled out from cement paste by slowly increasing load cycles, Cem. Concr. Compos 134 (2022) 104799, https://doi.org/10.1016/j.cemconcomp.2022.104799.
[34] J. Cid, F.R. Mazarrón, I. Cañas, Las normativas de construcción con tierra en el mundo, Inf. Constr. 63 (2011) 159–169. https://informesdelaconstruccion.revistas.csic.es/index.php/informesdelaconstruccion/article/view/1262.
[35] Norma e.080 Diseño y Construcción con Tierra Reforzada, Ministerio de Vivienda Construccion y Saneamiento - Mexico, (2017), https://procurement-notices.undp.org/view_file.cfm?doc_id=109376.
[36] J. Qi, Y. Yao, J. Wang, F. Han, J. Lv, Effect of sand grain size and fibre size on macro – micro interfacial bond behavior of steel fibres and UHPC mortars, Mag. Concr. Res. 73 (2021) 228–239, https://doi.org/10.1680/jmacr.19.00099.
[37] O. Hurtado-figueroa, A.C. Escamilla, H. Varum, R.J. Gallardo, Effect of cassava starch, hydrated lime, and carboxymethylcellulose on the physicomechanical behavior of mixtures with clay matrix, Case Stud. Constr. Mater 20 (2024) e03022, https://doi.org/10.1016/j.cscm.2024.e03022.
[38] ASTM C307.23, Standard test method for tensile strength of chemical-resistant mortar, grouts, and monolithic surfacings, (2023) 1–3, https://www.astm.org/c0307-18.html.
[39] H. Omrani, L. Hassini, A. Benazzouk, H. Beji, A. Elcafsi, Elaboration and characterization of clay-sand composite based on Juncus acutus fibers, Constr. Build. Mater. 238 (2020) 117712, https://doi.org/10.1016/j.conbuildmat.2019.117712.
[40] M. Syed, A. Guharay, Effect of natural fiber reinforcement on strength response of alkali activated binder treated expansive soil : experimental investigation and reliability analysis, Constr. Build. Mater. 273 (2021) 121743, https://doi.org/10.1016/j.conbuildmat.2020.121743.
[41] Y. Li, F. Liu, H. Li, X. Zhang, Y. Pan, C. Liu, Pullout behavior of single arc-shaped steel fiber from brittle SIFCON matrix with various embedment lengths and inclination angles, Constr. Build. Mater 420 (2024) 135479, https://doi.org/10.1016/j.conbuildmat.2024.135479.
[42] D.W. Menna, A.S. Genikomsou, M.F. Green, Effect of heat treatment and end-hook geometry on pullout behaviour of heavily cold worked superelastic NiTi shape memory alloy fibres embedded in concrete, Constr. Build. Mater. 361 (2022) 129630, https://doi.org/10.1016/j.conbuildmat.2022.129630.
[43] J.D. Pardo, R.A. Robayo, L.A. Trejos, S.D. Arjona, Lightweight composites based on gypsum with reinforcement of rice husk and polystyrene, Inf. Téc. 79 (2015) 26–32. https://dialnet.unirioja.es/servlet/articulo?codigo=5290925.
[44] A. Pearson, W. Liao, Y. Kazemi, M. Duncan, E. Slingerland, A. Kakroodi, et al., Fiber-matrix adhesion between high-density polyethylene and carbon fiber, Polym. Test. 105 (2022) 107423, https://doi.org/10.1016/j.polymertesting.2021.107423.
[45] S. Zhang, S. He, B. Ghiassi, K.V. Breugel, G. Ye, Interface bonding properties of polyvinyl alcohol (PVA) fiber in alkali-activated slag/fly ash, Cem. Concr. Res. 173 (2023) 107308, https://doi.org/10.1016/j.cemconres.2023.107308.
[46] V. Fiore, G.D. Bella, A. Valenza, The effect of alkaline treatment on mechanical properties of kenaf fibers and their epoxy composites, Compos. B Eng. 68 (2015) 14–21, https://doi.org/10.1016/j.compositesb.2014.08.025.
[47] J.H. Park, J.H. Lee, E. Choi, C. Park, Effects of double-arched geometry and tensile strength on the pullout resistance of fibers, Case Stud, Constr. Mater. 19 (2023) e02316, https://doi.org/10.1016/j.cscm.2023.e02316.
[48] C. Lin, T. Kanstad, S. Jacobsen, G. Ji, Bonding property between fiber and cementitious matrix: a critical review, Constr. Build. Mater. 378 (2023) 131169, https://doi.org/10.1016/j.conbuildmat.2023.131169.
[49] A.B. Rezaie, M. Liebscher, M. Mohammadi, A. Drechsler, R. Frenzel, A. Synytska, et al., Influence of sodium periodate-accelerated polydopamine modification of polyethylene fibers on fiber-matrix bonding in cementitious composites, Cem. Concr. Compos. 152 (2024) 105601, https://doi.org/10.1016/j.cemconcomp.2024.105601.
[50] P. Chindaprasirt, P. Jamsawang, P. Sukontasukkul, P. Jongpradist, S. Likitlersuang, Comparative mechanical performances of cement-treated sand reinforced with fiber for road and pavement applications, Transp. Geotech. 30 (2021) 100626, https://doi.org/10.1016/j.trgeo.2021.100626.
[51] M.M. Kabir, H. Wang, K.T. Lau, F. Cardona, Tensile properties of chemically treated hemp fibres as reinforcement for composites, Compos. B Eng. 53 (2013) 362–368, https://doi.org/10.1016/j.compositesb.2013.05.048.
[52] L. Prabhu, V. Krishnaraj, S. Sathish, S. Gokulkumar, N. Karthi, L. Rajeshkumar, A review on natural fiber reinforced hybrid composites: chemical treatments, manufacturing methods and potential applications, Mater, Today Proc. 45 (2021) 8080–8085, https://doi.org/10.1016/j.matpr.2021.01.280.
[53] B.A. Goodman, Utilization of waste straw and husks from rice production: a review, J. Bioresour. Bioprod. 5 (2020) 143–162, https://doi.org/10.1016/j.jobab.2020.07.001.
[54] T. Chompoorat, S. Likitlersuang, P. Buathong, P. Jongpradist, P. Jamsawang, Flexural performance and microstructural characterization of cement-treated sand reinforced with palm fiber, JMR&T 25 (2023) 1570–1584, https://doi.org/10.1016/j.jmrt.2023.06.036.
[55] A. Alioui, S.I. Kaitouni, Y. Azalam, N. Al armouzi, E.M. Bendada, M. Mabrouki, Effect of straw fibers addition on hygrothermal and mechanical properties of carbon-free adobe bricks: from material to building scale in a semi-arid climate, Build. Environ. 255 (2024) 111380, https://doi.org/10.1016/j.buildenv.2024.111380.
[56] A. Gholampour, T. Ozbakkaloglu, A review of natural fiber composites: properties, modification and processing techniques, characterization, applications, J. Mater. Sci. (2019), https://doi.org/10.1007/s10853-019-03990-y.